# Classification of Leftover Shrimp Feed Based on Lift Net Design Utilizing the k-Nearest Neighbors Algorithm

Ahmad Hannan Asy-Syaf'ie[1], Agus Indra Gunawan[1,*], Setiawardhana[2] , Muhammad Edy Hidayat[3], Muhammad Andi Kurniawan[4]

[1]Department of Electrical Engineering, Politeknik Electronika Negeri Surabaya, Surabaya, Indonesia

[2]Department of Informatic and Computer Engineering, Politeknik Electronika Negeri Surabaya, Surabaya, Indonesia

[3]Departement of Mechatronics Engineering, Politeknik Bosowa, Makassar, Indonesia

[4]PT. Lumbung Nusantara Nastiti, Lampung, Indonesia

Received 30 April 2025; received in revised form 04 September 2025; accepted 10 September 2025

DOI: https://doi.org/10.46604/aiti.2024.15095

## Abstract

An effective Feeding Management System (FMS) is crucial in shrimp farming, as both overfeeding and underfeeding can adversely affect shrimp growth. To ensure optimal nutrition, an accurate FMS must account for factors such as shrimp size, weight, age, and leftover feed. This study presents a method for detecting leftover shrimp feed using custom-designed lift nets equipped with paired ultrasonic sensors. Two critical aspects are examined: the optimal timing for measurement and the ideal placement of the transmitter. Results show that measurements should be taken within 10 minutes of feed immersion to avoid feed disintegration. Additionally, placing the transmitter on the outer side of the lift net improves measurement accuracy. Ultrasonic echoes are analyzed to classify leftover feed using the k-Nearest Neighbors algorithm. Root Mean Square voltage-based classification effectively groups leftover feed into five classes, highlighting its potential to improve aquaculture feed management.

**Keywords:** feeding management, ultrasonic, k-NN, shrimp, aquaculture

## 1. Introduction

Shrimp farming represents a promising strategy for enhancing food security in Indonesia [1], with Vannamei shrimp being the most widely cultivated species [2-5]. Reports from the regional marine and fisheries department show that 70-80% of farms still rely on traditional methods, creating opportunities to shift toward more intensive and efficient systems. The transformation toward modernized aquaculture requires technology integration and skilled farmers supported by data-driven decision-making. A crucial element is the Feeding Management System (FMS), which regulates feed quantity based on shrimp species, size, age, population density, and environmental conditions [6-8]. Proper feeding prevents stunted growth, waste, and environmental degradation. Conventional methods often face challenges in accurately identifying leftover feed, as manual methods are subjective and imprecise. Therefore, the ability to detect feeding imbalances by analyzing leftover feed is essential for improving the effectiveness of FMS in modern shrimp aquaculture. Traditionally, shrimp farmers place 0.5%-1% of the total feed into a lift net and check leftover feed after a few minutes. But this process is inefficient and prone to error.

Studies on the detection of leftover shrimp feed in pellet form using image processing techniques were conducted in 2021 and 2023 [9-10]. This approach is feasible due to the floating position of the leftover feed, which enables visual capture using a camera, followed by computational image processing. In the same year [11], quantification of leftover shrimp feed in the

* Corresponding author. E-mail address: agus_ig@pens.ac.id

form of sinking pellets was also undertaken. In this case, the camera was able to detect the submerged feed due to the clear water conditions in the cultivation pond.

In the context of detecting leftover feed in shrimp ponds, neither of the aforementioned conditions is ideal. Shrimp ponds typically exhibit turbid water characteristics, and the coloration of the water often closely resembles that of pellet feed. These factors significantly reduce the accuracy of camera-based detection methods for identifying leftover shrimp feed. This limitation highlights the need for alternative sensing approaches capable of operating effectively under such challenging optical conditions.

Ultrasonic technology presents a promising solution, offering measurement capabilities that can address multi-layer material detection through wave penetration, even in opaque environments [12-14]. The echo signals generated from ultrasonic wave reflections can be processed and reconstructed to yield meaningful detection outputs. Based on the advantages of ultrasonic technology, the present study proposes the digitization of lift nets by redesigning their structure and incorporating multiple ultrasonic sensors. By leveraging ultrasonic wave propagation through water to detect the surfaces of solid materials (i.e., leftover feed), the system processes and classifies echo signals of ultrasonic waves to quantify the amount of uneaten shrimp feed. This approach is expected to overcome the limitations of optical detection methods.

This study proposes several lift net designs and identified the most optimal one for classifying leftover shrimp feed within the net. The classification of this residue is carried out using the k-Nearest Neighbors (k-NN) method. In the preliminary study, research was conducted under controlled laboratory conditions, which does not fully express the complexities of the actual operational environment. Consequently, certain environmental factors such as water speed and turbidity, and the existence of shrimp inside the liftnet are not incorporated into the study. These limitations may affect the direct applicability of the results to real-world scenarios. Therefore, future research should focus on validating the proposed system under actual field conditions to ensure its effectiveness and robustness in practical aquaculture operations.

## 2. Materials and Configuration

This section describes the materials and components used in the proposed system. These include shrimp feed, ultrasonic sensors, conventional lift nets, and electronic components. A detailed explanation is also provided for the custom-designed lift net, which replaces the function of traditional lift nets in this system.

### *2.1. Shrimp Feed*

To promote optimal shrimp growth, Artificial feed with high nutritional value is essential to ensure rapid and healthy shrimp growth. Fig. 1 displays one of the commercial shrimp feeds used in this study. From left to right, it shows 3S as a small type, 3M as a medium type, and 3L as a large type. The feed is pelletized, with sizes varying according to the shrimp's age and size. As the shrimp mature, the pellet size is adjusted to accommodate their growth.


Fig. 1 Shrimp feed

### *2.2. Ultrasonic Sensor*

Ultrasonic sensors generate high-frequency mechanical waves above 20 kHz and are widely used in applications such as distance measurement, cleaning, industrial automation, and medical diagnostics [15-18]. Distance measurement with ultrasonic sensors can be conducted using either reflection or transmission methods. In the reflection method, a single piezoelectric transducer emits ultrasonic waves, which are reflected by a target object and received by the same or a different transducer. In the transmission method, two transducers are used—one as a transmitter and the other as a receiver—positioned directly opposite each other. Fig. 2 shows the waterproof ultrasonic sensors used in this study.

Fig. 2 Waterproof ultrasonic sensors

### *2.3. Lift Net*

The lift net, illustrated in Fig. 3, also known as Anco (in Indonesia), is widely used in shrimp farming to monitor shrimp growth and manage feed. Typically shaped as a square or circular lift net, it is mounted on a rust-resistant frame made of stainless steel or bamboo. Although simple in design, the lift net plays a critical role in modern shrimp farming. Its consistent use contributes to successful harvests and optimal production.

Fig. 3 Conventional lift net

In this study, the conventional lift net was digitized while retaining its core function of monitoring leftover feed. To determine the most effective design for feed detection, four models were compared and fabricated using 3D printing with PLA material, as shown in Fig. 4. Each structure underwent sealing and painting, while the bottom was modified by attaching a mesh to prevent feed loss. Fig. 4(a) and 4(b) represent conical-shaped lift nets, while Fig. 4(c) and 4(d) represent pyramid-shaped designs.

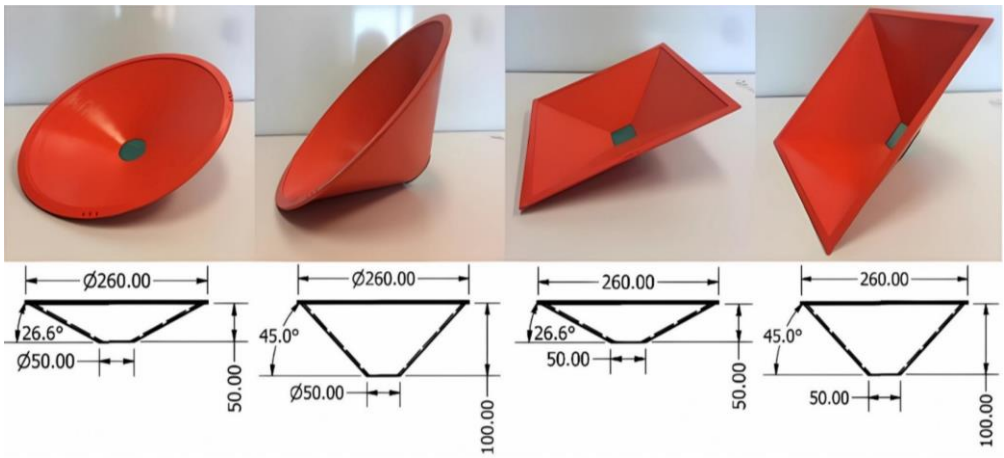


(a) Conical 5 cm (b) Conical 10 cm (c) Pyramid 5 cm (d) Pyramid 10 cm

Fig. 4 Portable lift net prototypes

To facilitate feed measurement, nine pairs of ultrasonic sensors were mounted on the top section of the lift net. Each pair consists of one transmitter and one receiver. The sensors are strategically positioned as follows: one pair at the pos-1 (shown by number 9), four pairs at the pos-2 region (shown by numbers 5, 6, 7, and 8), and four pairs at the pos-3 (shown by numbers 1, 2, 3, and 4), as illustrated in Fig. 5.

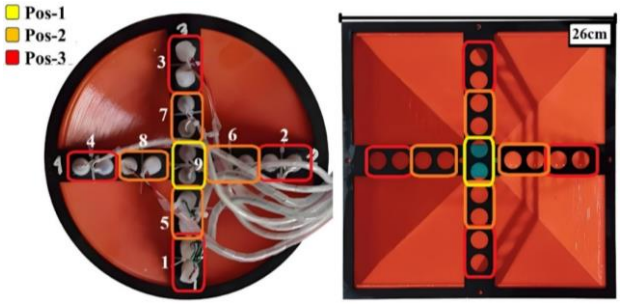


Fig. 5 Sensor placement on the lift net

### *2.4. Electronic Module*

The electronic module of the system is depicted in Fig. 6. This section comprises a power supply unit, amplifier, relays, a microcontroller, and ports for connecting the electronic module to the ultrasonic sensors at the lift net. A 35 kHz acoustic signal is generated by the microcontroller, and then it is amplified before being transmitted to the ultrasonic sensors. The microcontroller also controls which sensors are active by switching the corresponding relays on and off. With this control mechanism, the ultrasonic sensors work alternately, thereby reducing echo signal interference between sensors.

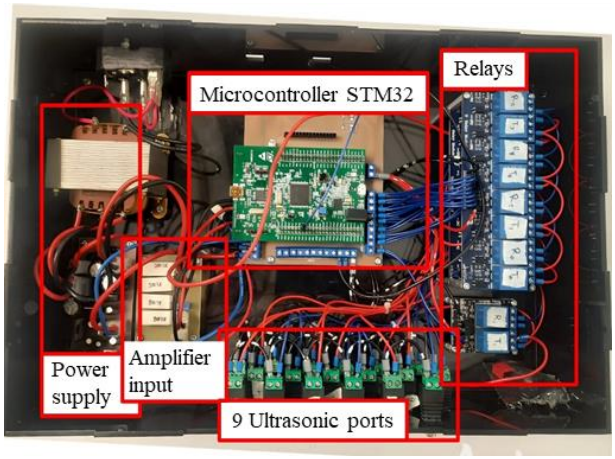


Fig. 6 Electronic components

## 3. Research Methodology

This chapter outlines the research methodology, including the proposed system, the measurement concept, and the classification method. The proposed system, comprising the electronic components and lift net, is described in detail. Additionally, this section explains how the measurements are set up, how echo signals are acquired and processed, and how the data is analyzed using the k-NN algorithm.

### *3.1. The Proposed System*

Fig. 7(a) illustrates the proposed system comprising an electronic module, a lift net, and ultrasonic sensors, while Fig. 7(b) shows its block diagram. During the measurement process, the ultrasonic sensors, liftnet, and feed are immersed in water. In the hardware section, a microcontroller generates a 35 kHz signal for the transmitter (Tx), which converts it into an acoustic signal. The microcontroller also selects the active pair of ultrasonic sensors to work alternately to minimize echo interference.

This acoustic signal travels through the water until it reaches the feed or the lift net frame and is received by the receiver (Rx), which converts it back into an electrical signal. These signals are then acquired by the microcontroller and processed on a computer.

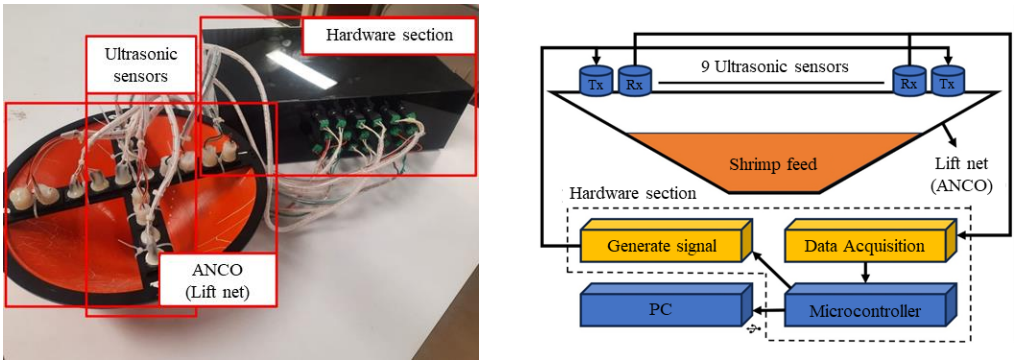


(a) Overall system (b) Block diagram system

Fig. 7 The proposed system

### *3.2. Measurement Method*

The classification of leftover shrimp feed is based on the analysis of echo signals. The echo signals provide two parameters: time of flight (ToF) and signal magnitude, which is represented in voltage. Fig. 8(a) illustrates the measurement of one-dimensional space using these parameters. When a trigger signal is emitted by the transmitter ultrasonic sensor, the receiver ultrasonic sensor detects the returning echo. The blue echo ($Echo_{blue}$) refers to the signal reflected from the surface of the feed. It provides the time of flight for the blue echo signal ($ToF_{blue}$) and its magnitude, measured using Root Mean Squared (RMS) and peak-to-peak voltage. The red echo ($Echo_{red}$) is the signal reflected from the lift net frame, serving as a reference. It provides ($ToF_{red}$) and its respective magnitude values as well. Once both ($ToF_{red}$) and ($ToF_{blue}$) are known, the distance ($d$) can be calculated using the difference between $d_2$ and $d_1$, as defined in Eq. (1) through Eq. (3).

$$d_2 = c \times \frac{ToF_{red}}{2} \tag{1}$$

$$d_1 = c \times \frac{ToF_{blue}}{2} \tag{2}$$

$$d = d_2 - d_1 \tag{3}$$

where c is the acoustic speed in the water. In this study, both Time of Flight (ToF) and signal magnitude were evaluated in terms of voltage measurements. Two modes of voltage representation were applied: peak-to-peak [19] and RMS [20]. Each of these modes provides specific strengths and limitations in the context of material characterization [21]. The peak-to-peak measurement reflects the voltage span between the maximum positive and negative signal excursions, thereby emphasizing the full dynamic range of the echo response. On the other hand, the RMS measurement represents the effective voltage, defined as the DC-equivalent value that produces the same average power dissipation across a load, and is therefore often considered more robust for energy-related analysis. The formula of RMS voltage is shown in Eq. (4).

$$Vrms = \sqrt{\frac{1}{T}\int_0^T v(t)^2 \, dt} \tag{4}$$

where $v(t)$ is the instantaneous voltage as a function of time, and $T$ is the period of the signal. The squared voltage values are integrated over one complete cycle and then averaged by dividing by $T$. Finally, the square root is applied to obtain the RMS value. This calculation provides the effective voltage of an AC signal, which is equivalent to the DC voltage that would deliver the same power to a resistive load.

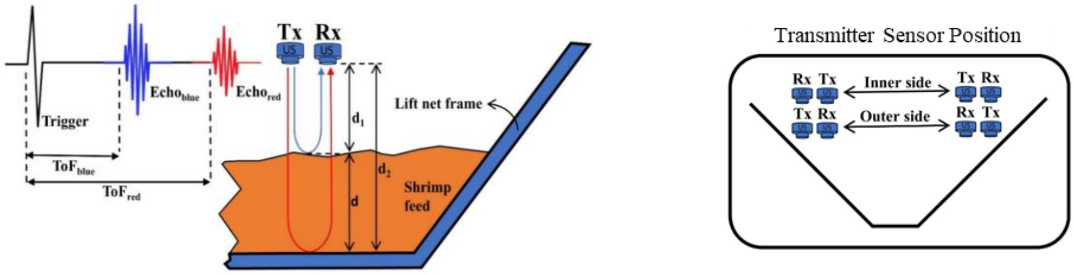


(a) Measurement concept (b) Transmitter (Tx) placement

Fig. 8 Measuring the lift net frame as a reference signal

The ToF was used to compare two transmitter positions: inner and outer side positions using an empty lift net, as shown in Fig. 8(b). Alternatively, the one-dimensional space ($d$) can be estimated from the $Echo_{blue}$ magnitude, where smaller values indicate longer travel distances. Thus, either the ToF or the voltage magnitude approach can be used to calculate or predict ($d$). Once the echo signal is obtained, it's processed by extracting features such as RMS and peak-to-peak voltage, and then used for classification and comparison using the k-NN algorithm.

### *3.3. Classification Method*

Measurements were carried out for five different feed quantities: 0 g, 50 g, 100 g, 150 g, and 200 g. In the initial phase, data acquisition was conducted in an aquarium to record echo signals from leftover feed placed in the lift net under simplified conditions, excluding turbidity, flow dynamics, and shrimp presence, as shown in Fig. 9. The feed was placed inside the lift net and submerged in water. In this study, each feed sample had a flat and circularly symmetric shape, and all experiments were conducted under ideal conditions in an aquarium (water tank), free from external disturbances.

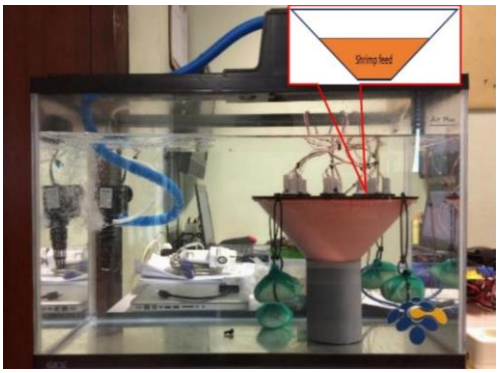


Fig. 9 Illustration of an experiment in an aquarium

The classification process was performed using the k-NN algorithm [22-24], which classifies the leftover feed into five categories based on the amount of leftover in the portable lift net. k-NN was chosen because it is simple, easy to implement, and suitable for small data sets [25]. A study comparing enhanced SVM and k-NN for IoT-based human activity recognition showed that k-NN achieved a higher average accuracy (97.08%) than SVM (95.88%) [26]. In this study, k-NN algorithm uses three input parameters to produce one output: the classification of leftover feed in the lift net. The sensor at the pos-1 is represented by the z-axis, sensors in the pos-2 are represented by the y-axis, and sensors on the pos-3 side are represented by the x-axis. Distance in the k-NN ($d_{knn}$) can be calculated by using the Euclidean method, as shown by Eq. (5):

$$d_{knn} = \sqrt{(x_n - a_x)^2 + (y_n - a_y)^2 + (z_n - a_z)^2} \tag{5}$$

where $x_n$, $y_n$, and $z_n$ are the attributes of the training data (learning data), and $a_x$, $a_y$, and $a_z$ are the attributes of the test data. The distance ($d_{knn}$) represents the distance between a test data point and one point in the training dataset. The distance calculation

is repeated for all available training data. The value of k in the k-NN algorithm influences the probability that a particular class will be selected as the final classification result. It determines how many of the closest data points are considered when estimating the class of a test sample.

## 4. Results and Discussion

This chapter presents the results and discussion of the measurements, including the condition of the feed when submerged in water, sensor position analysis, and feed measurement in the lift net using four different types of lift nets. The analysis is performed using the k-NN algorithm. The objective is to determine the most suitable lift net model for measuring the leftover shrimp feed.

### *4.1. Shrimp Feed Dissolution Time in Water*

In this study, Dissolution times for three shrimp feed types (3S, 3M, 3L) were measured (Fig. 1), as feed gradually dissolves depending on its type and composition. Once the dissolution time was determined, all measurements were conducted within the determined dissolution time to ensure accuracy, using locally available feed. Experiments assumed that zero water flow and no shrimp were present in the lift net, so there was no need to differentiate echo signals from the feed and those from shrimp. Experiments were conducted under two conditions: still water and moving water. Observations were recorded every five minutes, up to a maximum of 30 minutes.

(a) 1 minute (b) 15 minutes (c) 30 minutes

Fig. 10 Shrimp feed (3L) condition over time

Table 1 shows the condition of each shrimp feed type in water (sturdy, rather sturdy, and fragile) over time, indicating that leftover feed measurements are best conducted within 10 minutes before degradation to the “rather sturdy” condition. Fig. 10 shows 3L shrimp feed after immersion in still water. Sturdy condition is shown in Fig. 10(a) after 1 minute immersion, and rather sturdy and fragile conditions are shown in Fig. 10(b) and Fig. 10(c) after 15 minutes and 30 minutes immersion, respectively. Still water was used to ensure image clarity, avoiding turbidity from water movement.

Table 1 Shrimp feed condition over time

| Shrimp Feed Size | Water Condition | Feed Condition (Minutes) | | |
|---|---|---|---|---|
| | | Sturdy | Rather Sturdy | Fragile |
| 3S | Still | 0-15 | 15-25 | >25 |
| | Moving | 0-10 | 10-20 | >20 |
| 3M | Still | 0-20 | 20-25 | >25 |
| | Moving | 0-15 | 15-20 | >20 |
| 3L | Still | 0-25 | 25-30 | >30 |
| | Moving | 0-20 | 20-30 | >30 |

### *4.2. Sensor Position Analysis*

This section presents additional experiments to determine distance information based on echo signals with the lift net empty. As shown in Fig. 8, two transmitter (Tx) positions were tested: one placed on the outer side (farther from the center of the lift net) and one placed on the inner side (closer to the center). Only pos-2 and pos-3 ultrasonic sensor regions were used,

since pos-1 is equidistant from Tx and Rx and thus unaffected by transmitter placement. To determine the distance between the sensor surface and the lift net frame, Eq. (1) was used, with *c*, the speed of sound in freshwater, approximated at 1480 m/s. The experimental results are presented in Table 2.

Table 2 Comparison of distance measurement results

| Transmitter Position | Portable Lift Net Type/Height | Sensor Position | Actual Distance (cm) | Calculated Distance (cm) | % Error |
|---|---|---|---|---|---|
| Inner side | Conical/ 5cm | Pos-2 | 4.8 | 5.426124 | 13.04 |
| | | Pos-3 | 2.8 | 3.206346 | 14.51 |
| | Conical/ 10cm | Pos-2 | 9.2 | 9.86568 | 7.23 |
| | | Pos-3 | 5 | 5.426124 | 8.52 |
| | Pyramid/ 5cm | Pos-2 | 4.8 | 5.179482 | 7.90 |
| | | Pos-3 | 2.8 | 3.69963 | 32.12 |
| | Pyramid/ 10cm | Pos-2 | 9.2 | 10.112322 | 9.91 |
| | | Pos-3 | 5 | 5.672766 | 13.45 |
| Outer side | Conical/ 5cm | Pos-2 | 4.8 | 4.93284 | 2.76 |
| | | Pos-3 | 2.8 | 2.713062 | 3.10 |
| | Conical/ 10cm | Pos-2 | 9.2 | 9.125754 | 0.80 |
| | | Pos-3 | 5 | 4.93284 | 1.34 |
| | Pyramid/ 5cm | Pos-2 | 4.8 | 4.686198 | 2.37 |
| | | Pos-3 | 2.8 | 3.452988 | 23.32 |
| | Pyramid/ 10cm | Pos-2 | 9.2 | 9.619038 | 4.55 |
| | | Pos-3 | 5 | 5.179482 | 3.58 |

In ultrasonic propagation, the near and far fields influence wave behavior, which is critical for sensing leftover feed or the lift net frame. However, since the diameter of the sensor is 10 mm and the wavelength (λ) is 37 mm, it means the diameter of an ultrasonic sensor is less than or equal to λ, causing diffraction and near-omnidirectional beam spread. In this scenario, the relatively small aperture leads to significant beam divergence, causing the ultrasound waves to propagate widely in all directions [27-28]. This omnidirectional behavior is further influenced by the relationship between wavelength and frequency, where longer wavelengths contribute to a broader beam spread. As shown in Table 2, placing the transmitter on the outer side yields more accurate measurements than the inner side. These results are also visualized in Fig. 11. Among all configurations, the conical-shaped lift net (5 cm and 10 cm height) provides the highest measurement accuracy. From the measurement, the 5 cm conical-shaped lift net showed an error of 2.76% at Post-2 and 3.10% at Post-3. Meanwhile, the 10 cm conical-shaped lift net achieved a lower error of 0.8% at Post-2 and 1.34% at Post-3.

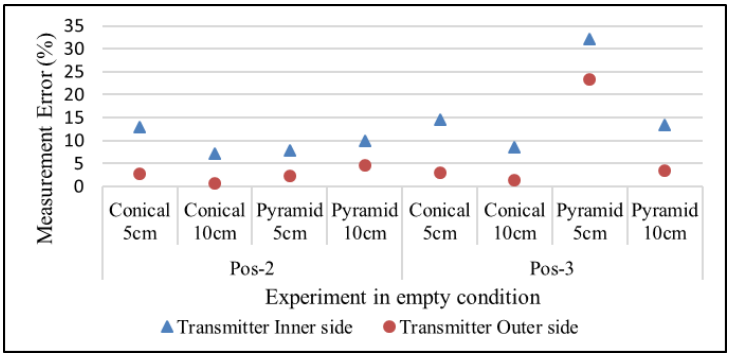


Fig. 11 Comparison of measurement errors

According to Fig. 12, the lift net frame is represented by the solid black line, ultrasonic propagation by blue and red lines, and the normal line by the red dashed line, which is perpendicular to the lift net frame. As illustrated in Fig. 12(a) and Fig. 12(b), it can be seen that when the transmitter is positioned at the inner side, the frame tilt directs the signal away from the receiver and makes it more difficult to detect, resulting in weaker detection. Conversely, as shown in Fig. 12(c) and Fig. 12(d), positioning the transmitter on the outer side directs the signal toward the receiver, as shown by solid red lines. Thereby, this configuration improves measurement accuracy.

Additionally, a comparison between the conical-shaped and pyramid-shaped lift net designs in Fig. 11 reveals that the conical-shaped lift net achieves higher measurement accuracy. This advantage is attributed to the conical-shaped frame's ability to concentrate the echo signals, producing stronger received signals and enhancing resistance to noise disturbances.

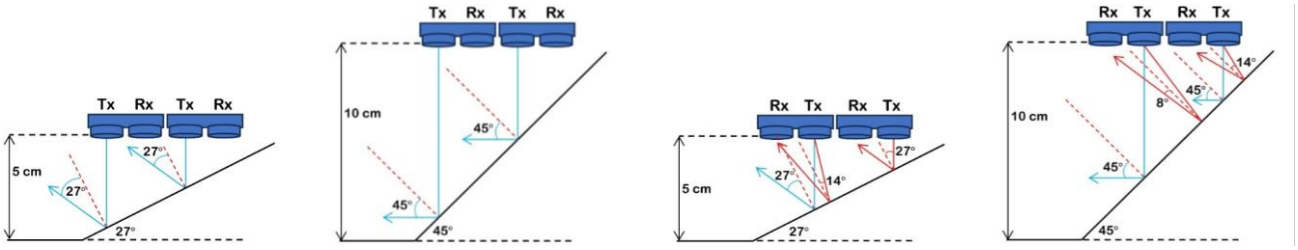


(a) Inner side for 5 cm (b) Inner side for 10 cm (c) Outer side for 5 cm (d) Outer side for 10 cm

Fig. 12 Propagation analysis of ultrasonic signal based on transmitter position.

### *4.3. Shrimp Feed Measurement Inside the Lift Net*

This section presents the results of shrimp feed measurements conducted inside four different lift nets: a conical-shaped net with heights of 5 cm and 10 cm, and a pyramid-shaped net with heights of 5 cm and 10 cm. For each lift net type, five feed weight classes were defined as references for the leftover feed inside the lift net: 0 g, 50 g, 100 g, 150 g, and 200 g. A total of 125 measurements were performed, with 100 data points used for training and 25 data points used for validation. When an ultrasonic signal is emitted by the transmitter, it propagates through the water, reflects off the shrimp feed, and is received by the receiver ultrasonic sensor. The resulting echo is analyzed based on RMS voltage and peak-to-peak voltage. In this study, four k values (1, 3, 5, and 7) are used to obtain the most suitable for the accuracy of classification.

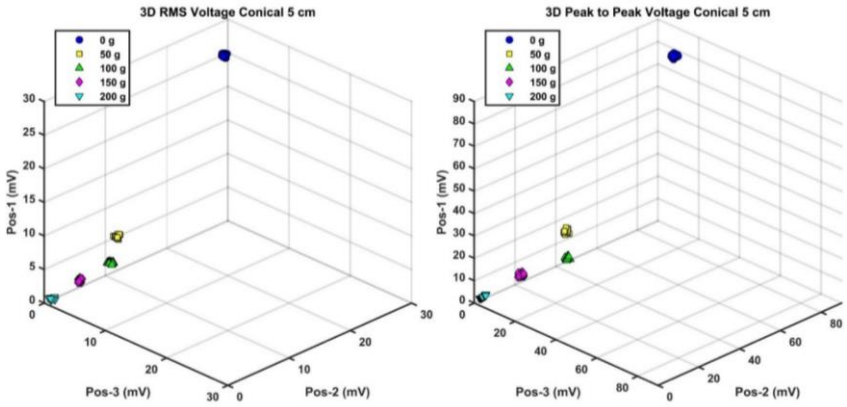


Fig. 13 Data plot from measurement using a 5 cm conical-shaped lift net

Fig. 13 shows a plot of the data from measurements using a 5 cm conical-shaped lift net. To assess the success of the classification, 25 new data points based on measurements were tested using Eq. (5). The results of this test are presented in Table 3.

Table 3 RMS and peak-to-peak voltage measurements using a 5 cm conical-shaped lift net

| Class | RMS Voltage | Peak -Peak Voltage |
|---|---|---|
| 0 g | All K values are correct | All K values are correct |
| 50 g | All K values are correct | All K values are correct |
| 100 g | All K values are correct | All K values are correct |
| 150 g | All K values are correct | All K values are correct |
| 200 g | All K values are correct | All K values are correct |

Similarly, the data plots obtained from experimental measurements using the 10 cm conical-shaped lift net, the 5 cm pyramid-shaped lift net, and the 10 cm pyramid-shaped lift net are clearly presented and compared in Figs. 14-16, respectively.

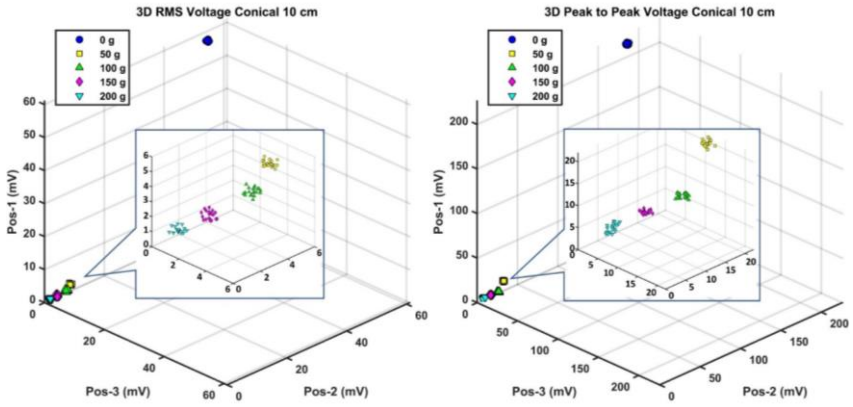


Fig. 14 Data plot from measurements using a 10 cm conical-shaped lift net

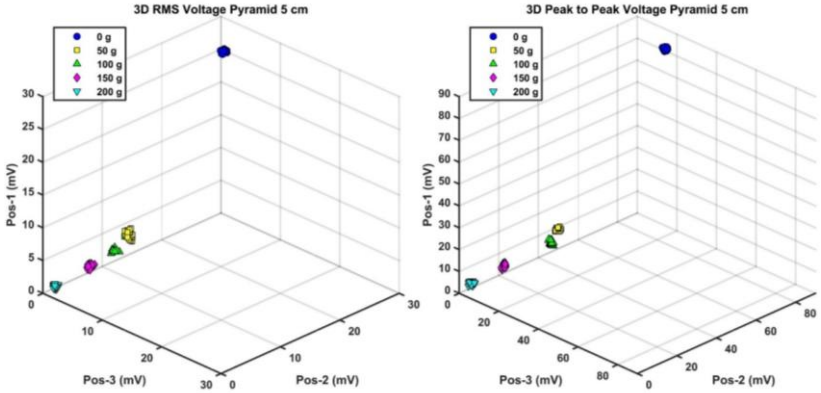


Fig. 15 Data plot from measurements using a 5 cm pyramid-shaped lift net

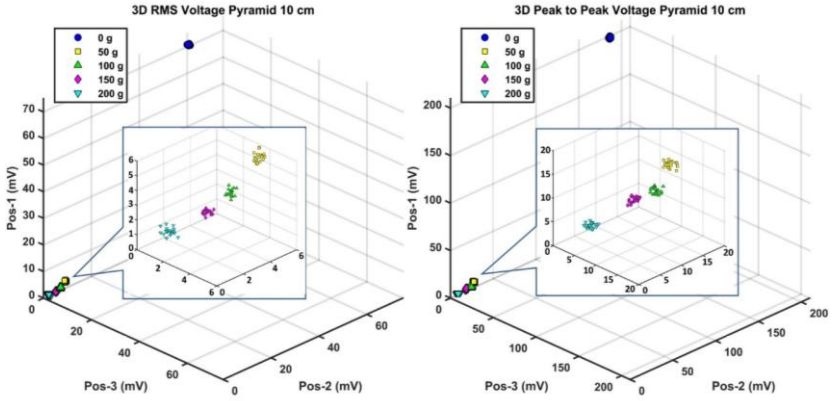


Fig. 16 Data plot from measurements using a 10 cm pyramid-shaped lift net

Once the classification based on weight was completed, testing was conducted using new data. The results of these tests are sequentially presented in Tables 4-6, which show the test outcomes for a 10 cm conical-shaped lift net, a 5 cm pyramid-shaped lift net, and a 10 cm pyramid-shaped lift net, respectively.

Table 4 RMS and peak-to-peak voltage measurements using a 10 cm conical-shaped lift net

| Class | RMS Voltage | Peak-to-Peak Voltage |
|---|---|---|
| 0 g | All K values are correct | All K values are correct |
| 50 g | All K values are correct | For K = 3, 1 neighbor is false<br>For K = 5, 3 neighbors are false<br>For K = 7, 4 neighbors are false |
| 100 g | All K values are correct | All K values are correct |
| 150 g | All K values are correct | All K values are correct |
| 200 g | All K values are correct | All K values are correct |

Table 5 RMS and peak-to-peak voltage measurements using a 5 cm pyramid-shaped lift net

| Class | RMS Voltage | Peak-to-Peak Voltage |
|---|---|---|
| 0 g | All K values are correct | All K values are correct |
| 50 g | All K values are correct | All K values are correct |
| 100 g | All K values are correct | All K values are correct |
| 150 g | All K values are correct | All K values are correct |
| 200 g | All K values are correct | All K values are correct |

Table 6 RMS and peak-to-peak voltage measurements using a 10 cm pyramid-shaped lift net

| Class | RMS Voltage | Peak-to-Peak Voltage |
|---|---|---|
| 0 g | All K values are correct | All K values are correct |
| 50 g | All K values are correct | All K values are correct |
| 100 g | All K values are correct | All K values are correct |
| 150 g | All K values are correct | All K values are correct |
| 200 g | All K values are correct | All K values are correct |

Based on the classification results from the voltage plots, both the RMS and peak-to-peak voltage, the 5 cm lift net provides better classification accuracy. This is evident from the plots, where the leftover feed for 5 weight classes forms distinct groups based on weight. The deviation within each group is minimal, reducing the potential for overlap.

Conversely, for the 10 cm lift net, the leftover feed for 5 weight classes tends to cluster more closely together. Although the deviation within each group remains insignificant, the shorter distance between classes results in reduced classification accuracy, particularly when measurement issues, such as noise interference, occur. This can be observed in Table 4, where some inaccuracies were noted in the measurements for the 10 cm conical-shaped lift net, particularly with peak-to-peak voltage.

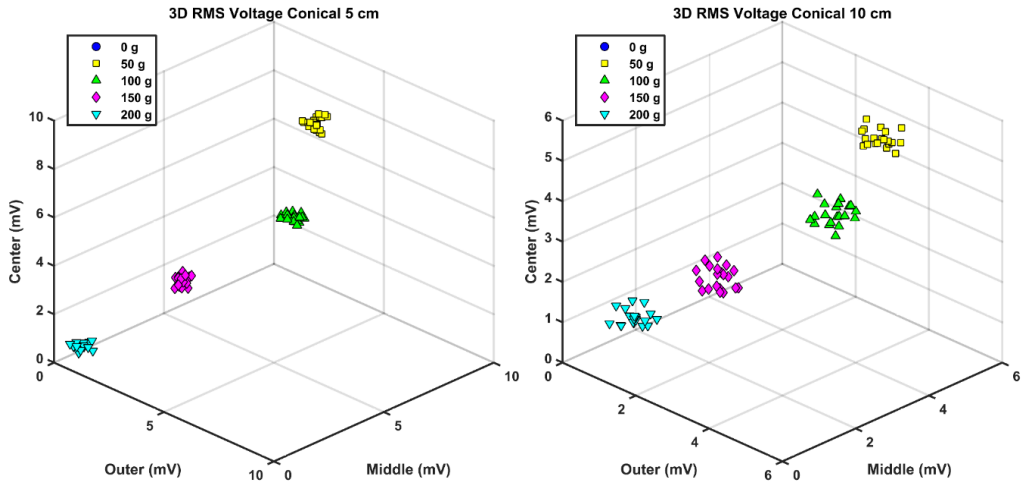


Fig. 17 Results of leftover feed classification using RMS voltage for 5 cm and 10 cm conical-shaped lift nets

Based on these results, the subsequent discussion will be focused on the measurement result using RMS voltage only. As shown in Subchapter 4.2, the transmitter positioned on the outer side outperforms the inner-side configuration, while the conical-shaped design of the lift net shows superior performance compared to the pyramid-shaped design. Moreover, the 10 cm conical-shaped lift net achieved higher accuracy than the 5 cm variant. Interestingly, these results appear to contrast with the k-NN classification presented in Subchapter 4.3, where the 5 cm conical-shaped lift net was shown to perform better than the 10 cm conical-shaped lift net. This argument is reinforced by the results shown in Fig. 17, where the k-NN classification using the 5 cm conical-shaped lift net demonstrates smaller deviations and greater inter-class separation compared to the 10 cm conical-shaped lift net. These characteristics imply that the classification errors with the 5 cm conical-shaped lift net are lower, therefore yielding higher accuracy than the 10 cm conical-shaped lift net.

### *4.4. Model Evaluation*

To strengthen the previous analysis, model evaluation was carried out using additional datasets for the 5 cm and 10 cm conical-shaped lift nets, focusing on the RMS voltage feature. The evaluation is presented in the form of classification reports and confusion matrices to demonstrate the classification performance of both models. Results of the classification report for the 5 cm conical-shaped lift net are shown in Table 7.

Table 7 Classification report for 5 cm conical-shaped lift net using RMS voltage

| Class | Precision | Recall | F1-score | Support |
|---|---|---|---|---|
| 0 g | 1.00 | 1.00 | 1.00 | 7 |
| 50 g | 1.00 | 0.82 | 0.90 | 11 |
| 100 g | 0.85 | 1.00 | 0.92 | 11 |
| 150 g | 1.00 | 1.00 | 1.00 | 15 |
| 200 g | 1.00 | 1.00 | 1.00 | 6 |
| Accuracy | | | 0.96 | 50 |
| Macro avg | 0.97 | 0.96 | 0.96 | 50 |
| Weighted avg | 0.97 | 0.96 | 0.96 | 50 |

The results show that classification using the 5 cm conical-shaped lift net achieved an accuracy of 96%, with precision, recall, and F1-scores above 0.82 across all classes, with very few misclassifications, mainly occurring in the 50 g classes. The results of the classification report for the 10 cm conical-shaped lift net are shown in Table 8. From these two tables, it can be seen that the performance of the 5 cm conical-shaped lift net is better than that of the 10 cm conical-shaped lift net.

Table 8 Classification report for 10 cm conical-shaped lift net using RMS voltage

| Class | Precision | Recall | F1-score | Support |
|---|---|---|---|---|
| 0 g | 1.00 | 1.00 | 1.00 | 7 |
| 50 g | 0.90 | 0.82 | 0.86 | 11 |
| 100 g | 0.83 | 0.91 | 0.87 | 11 |
| 150 g | 1.00 | 1.00 | 1.00 | 15 |
| 200 g | 1.00 | 1.00 | 1.00 | 6 |
| Accuracy | | | 0.94 | 50 |
| Macro avg | 0.95 | 0.95 | 0.95 | 50 |
| Weighted avg | 0.94 | 0.94 | 0.94 | 50 |

This conclusion is further supported by the confusion matrix analysis in Fig. 18, which consistently highlights the stronger performance of the 5 cm conical-shaped lift net. Therefore, for the task of classifying leftover shrimp feed, a conical-shaped lift net with a 5 cm height is recommended.

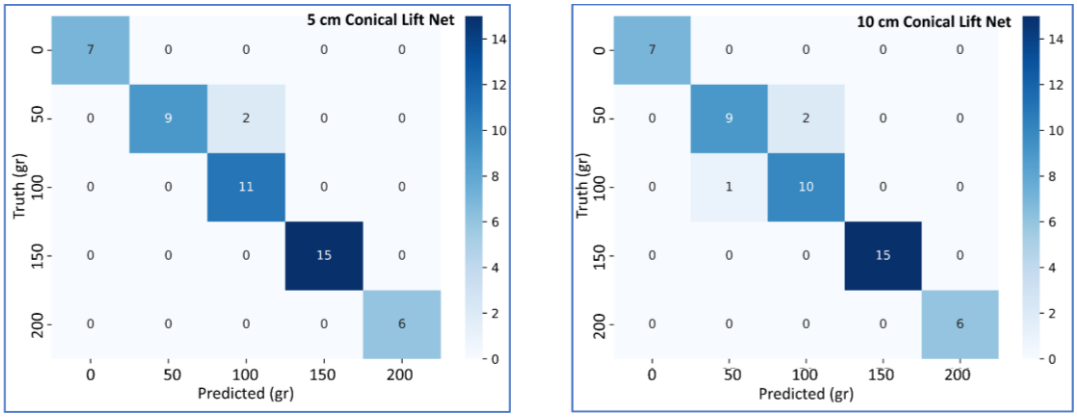


Fig. 18 Confusion matrix of RMS voltage for 5 cm and 10 cm conical-shaped lift nets

## 5. Conclusion

This study proposes and validates an ultrasonic-based method for quantifying leftover shrimp feed in a lift net. Four lift net designs were evaluated, each equipped with nine ultrasonic sensor pairs, and performance was further assessed using the k-NN classification algorithm with RMS voltage as the primary feature. The results demonstrate the feasibility of integrating ultrasonic sensing into an automated Feeding Management System (FMS).

The main conclusions are as follows:

(1) Measurements should be conducted immediately and within 10 minutes, as feed particles become fragile and deteriorate after prolonged water immersion.
(2) Transmitter sensors positioned on the outer side of the lift net exhibited superior performance, particularly when the net is empty.
(3) Among all tested designs, the 5 cm conical-shaped lift net achieved the highest accuracy.
(4) With RMS voltage as the classification feature, the k-NN algorithm achieved accuracies of 96% for the 5 cm conical-shaped lift net and 94% for the 10 cm version.
(5) The proposed system shows strong potential for classifying leftover feed and may serve as a foundation for integration into automated FMS in shrimp aquaculture.
(6) Future work should compare current results with the Time of Flight (ToF) technique or with volume estimation based on sensor positions.
(7) Additional experiments under turbid and flowing water conditions, along with tests involving shrimps inside the lift net, are recommended, as shrimps are likely to enter the net during feeding.

## Acknowledgment

The author would like to thank the Electrical Engineering for Aquaculture Technology Research Group, Politeknik Elektronika Negeri Surabaya, and PT. Lumbung Nusantara Nastiti, for providing support in terms of instruments, equipment, and laboratory facilities during this research.

## Conflicts of Interest

The authors declare no conflict of interest.

## References

[1] S. Bahri, D. Mardhia, and O. Saputra, “Growth and Graduation of Vannamei Shell Life (Litopenaeus Vannamei) with Feeding Tray (ANCO) System in AV 8 Lim Shrimp Organization (LSO) in Sumbawa District,” Jurnal Biologi Tropis, vol. 20, no. 2, pp. 279-289, 2020.
[2] E. P. Borges, L. P. Machado, A. C. Louza, A. C. Ramaglia, M. R. Santos, and A. Augusto, “Physiological Effects of Feeding Whiteleg Shrimp (Penaeus Vannamei) with the Fresh Macroalgae Chaetomorpha Clavata,” Aquaculture Reports, vol. 37, article no. 102222, 2024.
[3] C. E. Ullman, “An Evaluation of Feed Management, the Use of Automatic Feeders, and Feed Leaching in the Culture of Pacific White Shrimp Litopenaeus Vannamei,” Master Thesis, Department of Fisheries and Allied Aquacultures, Auburn University, Auburn, Alabama, 2017.
[4] I. Purnamasari, D. Purnama, and M. A. F. Utami, “Pertumbuhan Udang Vanname (Litopenaeus Vannamei) di Tambak Intensif,” Jurnal Enggano, vol. 2, no. 1, pp. 58-67, 2017.
[5] M. K. Amiin, A. F. Lahay, R. B. Putriani, M. Reza, S. M. E. Putri, M. A. A. Sumon, et al., “The Role of Probiotics in Vannamei Shrimp Aquaculture Performance - A Review,” Vet World, vol. 16, no. 3, pp. 638-649, 2023.
[6] J. Niu, X. Chen, Y. Q. Zhang, L. X. Tian, H. Z. Lin, et al., “The Effect of Different Feeding Rates on Growth, Feed Efficiency and Immunity of Juvenile Penaeus Monodon,” Aquaculture International, vol 24, no. 1, pp. 101-114, 2016.

[7] C. D. Powell, F. Tansil, J. France, and D. P. Bureau, "Growth Trajectory Analysis of Pacific Whiteleg Shrimp (Litopenaeus Vannamei): Comparison of the Specific Growth Rate, the Thermal-Unit Growth Coefficient and Its Adaptations," Aquaculture Research, vol. 51, no. 2, pp. 1-10, 2019.

[8] K. L. Oken, S. D. Groth, D. S. Holland, A. E. Punt, and E. J. Ward, "Variability in Somatic Growth Over Time and Space Determines Optimal Season-Opening Date in the Oregon Ocean Shrimp (Pandalus jordani) Fishery," Canadian Journal of Fisheries and Aquatic Sciences, vol. 82, pp. 1-13, 2024.

[9] M. G. B. Palconit, R. S. Conception II, J. D. Alejandrino, I. R. S. Evangelista, E. Sybingco, et al., "Counting of Uneaten Floating Feed Pellets in Water Surface Images using ACF Detector and Sobel Edge Operator," Proceedings IEEE 9th Region 10 Humanitarian Technology Conference (R10-HTC), pp. 1-5, 2021.

[10] Riyandani, I. Jaya, and A. Rahmat, "Computer Vision-Based Fish Feed Detection and Quantification System," Journal of Applied Geospatial Information, vol. 7, no. 1, pp. 832-839, 2023.

[11] C. Xu, Z. Wang, R. Du, Y. Li, D. Li, et al., "A Method for Detecting Uneaten Feed Based on Improved YOLOv5," Computers and Electronics in Agriculture, vol. 212, article no. 108101, 2023.

[12] F. Hagglund, J. Martinsson, and J. E. Carlson, "Model-Based Estimation of Thin Multi-Layered Media Using Ultrasonic Measurements," IEEE Transactions on Ultrasonics, Ferroelectrics, and Frequency Control, vol. 56, no. 8, pp. 1689-1702, 2009.

[13] F. P. Nurmaida, A. I. Gunawan, and R. S. Dewanto, "A Study of Acoustic Parameters of Transformer Oil Based on Its Water Content Utilizing a Single Ultrasonic Sensor," Advances in Technology Innovation, vol. 9, no. 3, pp. 186-196, 2024.

[14] R. Setiawan, A. Kusumadjati, N. S. Aminah, M. Djamal, and S. Viridi, "An Ultrasonic Sensor System for Vehicle Detection Application," Journal of Physics: Conference Series, vol. 1204, article no. 012017, 2019.

[15] S. Peixoto, R. Soares, and D. A. Davis, "An Acoustic Based Approach to Evaluate the Effect of Different Diet Lengths on Feeding Behavior of Litopenaeus Vannamei," Aquacultural Engineering, vol. 91, article no. 102114, 2020.

[16] L. Koval, J. Vanus, and P. Bilik, "Distance Measuring by Ultrasonic Sensor," IFAC-PaperOnLine, vol. 49, no. 25, pp. 153-158, 2016.

[17] A. Carullo and M. Parvis, "An Ultrasonic Sensor for Distance Measurement in Automotive Applications," IEEE Sensors Journal, vol. 1, no. 2, pp. 143-147, 2001.

[18] A. I. Gunawan, B. S. B. Dewantara, T. B. Santoso, I. D. Wicaksono, E. B. Prastika, and C. E. Prianto, "Characterizing Acoustic Impedance of Several Saline Solution Utilizing Range Finder Acoustic Sensor," Proceedings of International Electronics Symposium on Engineering Technology and Applications (IES-ETA), pp. 212-217, 2017.

[19] J. O. Smith, Spectral Audio Signal Processing, Stanford, CA: W3K Publishing, 2011.

[20] M. A. Richards, Fundamentals of Radar Signal Processing, 2nd ed. New York: McGraw-Hill, 2014.

[21] L. Xavier, An Introduction to Underwater Acoustics: Principles and Applications, 2nd ed., Springer Berlin, Heidelberg, 2010.

[22] M. Mohy-Eddine, A. Guezzaz, S. Benkirane, and M. Azrour, "An Efficient Network Intrusion Detection Model for IoT Security using K-NN Classifier and Feature Selection," Multimedia Tools and Applications, vol. 82, pp. 23615-23633, 2023.

[23] P. K. Syriopoulos, N. G. Kalampalikis, S. B. Kotsiantis, and M. N. Vrahatis, "KNN Classification: A Review," Annals of Mathematics and Artificial Intelligence, vol. 93, pp. 43-75, 2023.

[24] M. H. Yacoub, S. M. Ismail, L. A. Said, A. H. Madian, and A. G. Radwan, "Generic Hardware Realization of K Nearest Neighbors on FPGA," Proceedings of the 2022 International Conference on Microelectronics (ICM), pp. 169-172, 2022.

[25] N. Bhatia and Vandana, "Survey of Nearest Neighbor Techniques," International Journal of Computer Science and Information Security, vol. 8, No. 2, pp. 302-305, 2010.

[26] A. Y. Shdefat, N. Mostafa, Z. Al-Arnaout, Y. Kotb, and S. Alabed, "Optimizing HAR Systems: Comparative Analysis of Enhanced SVM and k-NN Classifiers," International Journal of Computational Intelligence Systems, vol. 17, article no. 150, 2024.

[27] T. L. Szabo, Diagnostic Ultrasound Imaging: Inside Out, Burlington, MA, USA: Academic Press, 2004.

[28] N. Kono and S. Hirose, "Semi-Analytical Modeling of Acoustic Beam Divergence in Homogeneous Anisotropic Half-Spaces," Ultrasonics, vol. 65, pp. 194-199, 2016.

Copyright© by the authors. Licensee TAETI, Taiwan. This article is an open access article distributed under the terms and conditions of the Creative Commons Attribution (CC BY-NC) license (https://creativecommons.org/licenses/by-nc/4.0/).